Application of three-dimensional resonant acoustic spectroscopy method to rock and building materials

Lev Ostrovsky
*Zel Technologies/NOAA Environmental Technology Laboratory, 325 Broadway, Boulder, Colorado 80305
and Institute of Applied Physics, Russian Academy of Sciences, Nizhny Novgorod, Russia*

Andrey Lebedev, Alexander Matveyev, Andrey Potapov, Alexander Sutin,
and Irina Soustova
Institute of Applied Physics, Russian Academy of Sciences, Nizhny Novgorod, Russia

Paul Johnson
Los Alamos National Laboratory, Los Alamos, New Mexico 87501

This paper presents the experimental and theoretical results of applying resonant acoustic spectroscopy (RAS) to determine elastic parameters and losses in such consolidated granular materials as rock and building bricks. First, the theoretical aspects of the RAS method are outlined. A computer code for the rectangular and cylindrical samples was developed and tested. The results of experiments on specimens of rock and ceramic brick are then described. Finally, a modification of the previously published RUS algorithm is presented which permits a significant reduction in computing time for elongated samples. © *2001 Acoustical Society of America.*
[DOI: 10.1121/1.1402255]

I. INTRODUCTION

Among the fundamental characteristics of crystalline and noncrystalline materials are their elastic constants. Knowledge of the elasticity tensor is very important, in particular, for geophysical applications, where elastic constants obtained from seismic data provide information about Earth's interior structure.[1] Elastic constants are determined as derivatives of the free elastic energy with respect to the components of strain tensor. In the linear approximation, when the elastic energy is quadratic in strain, the number of independent elements of elastic tensor C_{ijkl} is, in the general case, 21. Symmetries of a specific crystal group (or crack/pore distribution) further reduce the number of independent constants (e.g., 2 for an isotropic medium, 3 for a cubic symmetry, 5 for hexagonal, and 6 for tetragonal).

There exist various methods for measuring elastic constants. They are considered in detail, for example, in Refs. 2 and 3. Until recently, most often used have been the methods based on pulse propagation. However, along with an obvious simplicity, they have shortcomings associated with a relatively low preciseness. In particular, errors are associated with high-frequency sound scattering by grains in rock samples.[4] Another group is resonance methods based on the measurement of resonance frequencies of a sample and an inversion for its elastic parameters. Introduced as early as the 1960s–70s, they have attracted a broad interest relatively recently, with the development of computer data processing. These methods are known as resonant ultrasound spectroscopy, RUS. The method was designed first for samples of spherical geometry.[4] Later, with the advent of the numerical solutions to inverse problems, it became possible to analyze resonant frequencies of a sample of arbitrary geometry. In Ref. 3 it is stated that the RUS technique provides the highest accuracy for elastic moduli determination.

A typical algorithm of RUS is based on the Lagrangian approach: a basis of eigenfunctions is substituted into Lagrangian equations which leads to an eigenvalue problem. Since the infinite-dimensional eigenvalue problem cannot be solved in general, approximate variational methods such as the Rayleigh–Ritz algorithm are used which involve a finite set of basis functions. Then, some *M* approximate eigenvalues and the corresponding eigenfunctions are obtained. If the series of basis functions is chosen properly, the lower eigenvalues can be calculated quite accurately. For rectangular samples, products of Legendre polynomials are typically used as basis functions for displacement.

In later works, products of power functions were suggested as a basis. Visscher *et al.*[5] have pointed out that using basis functions of the form $x^l y^m z^n$ allows for a solution for samples of several different shapes (shells, bells, cylinders, eggs, potatoes, etc.). This approach is known as the "algorithm of Ming/Migliori/Visscher."

The RUS analysis algorithm requires that RUS measurements determine the natural frequencies of a sample with stress-free boundary conditions. Resonance oscillations are excited by one transducer. The second transducer measures the amplitude and phase of the sample's response. To obtain the desired accuracy, one must minimize sample loading by the transducers. Ohno[6] proposed a method to control such a loading: a rectangular sample was supported by transducers at its opposite corners. The corners were used for contact because the displacements have a maximum in these points. Unlike conventional ultrasonic pulse measurements where strong coupling between the transducer and the sample is needed, the RUS method is attractive in that the sample acts as a natural amplifier due to resonance with a gain equal to the quality factor, so that strong coupling with the source is not necessary.

In our study we used the RUS technique modified for

finding the complex elasticity tensor of large samples of structured materials such as rocks and ceramics. Because of the relatively low frequency range, this method is free of the shortcomings of impulse measurements such as local scattering from local inhomogeneities, at least when the macroscopic sample parameters are of interest, or the nondestructive testing is being performed. We also suggest a modification of the RUS algorithm to significantly reduce the computing time for prolate cylindrical bars often used in experiments. Due to the large size of the rock samples in contrast to most of RUS measurement in crystals, the frequency range for our measurements was between 1 and 40 kHz. Thus, instead of RUS (resonant ultrasound spectroscopy) we suggest the name RAS (resonant acoustic spectroscopy).

A first application of resonant spectroscopy to rock (granites) is described in the early work by Birch[4] who used a spherical sample and derived its elastic parameters. Hence, the present paper can be somewhat considered a development of Birch's work with the use of more recent RUS algorithms, different materials and specimen shapes. The code developed here is applicable for both rectangular and cylindrical sample geometries. Experimental verification of the code, including its modification for elongated samples, was performed for rectangular parallelepipeds. Workability of the modified code for thin cylindrical bars was tested by using asymptotic analytical solutions.

II. BASIC RELATIONS FOR THE RAS METHOD

A. General consideration

As mentioned above, RAS analysis is based on the use of the variational principle and the Rayleigh–Ritz method, i.e., an approximation of eigenvectors of variational equations by a proper set of basis functions.[3] We begin with outlining the direct problem: finding the resonance frequencies. Since the RUS algorithm is thoroughly described in, e.g., Ref. 3, here we omit all intermediate equations and concentrate on main results on which our program has been based and then on the specifics of long samples (subsection E). The most usable sets of basis functions for a cylindrical sample are products of exponents:[5]

$$\Psi_\nu(x_1,x_2,x_3)=\left(\frac{x_1}{R}\right)^{n_1}\left(\frac{x_2}{R}\right)^{n_2}\left(\frac{2x_3}{H}\right)^{n_3},$$
$$\nu=\{n_1,n_2,n_3\}, \qquad (1)$$

where R and H are the radius and the length of the cylinder, respectively. The basis Eq. (1) can also be used for the rectangular parallelepiped shape (for the sake of brevity, we shall occasionally refer to the latter as rectangular shape). For the analysis of our experiments with rectangular samples we shall use Legendre polynomials.[3] [However, in the last section we shall use the representation Eq. (1) as well]:

$$\Psi_\nu(x_1,x_2,x_3)=P_{n_1}\left(\frac{2x_1}{L_1}\right)P_{n_2}\left(\frac{2x_2}{L_2}\right)P_{n_3}\left(\frac{2x_3}{L_3}\right),$$
$$\nu=\{n_1,n_2,n_3\}, \qquad (2)$$

where L_j are sides of the parallelepiped.

The displacement vector **u** can be represented as a series:

$$u_i(x_1,x_2,x_3)=a_{i\nu}\Psi_\nu(x_1,x_2,x_3). \qquad (3)$$

The indexes n_1, n_2 and n_3 in Eq. (1) are chosen to provide integration inside the sphere

$$|k|\leqslant K \qquad (4)$$

in the wave number space. The value of K can be evaluated using a simple idea: $K=\max(\omega)/\min(V)$, where $\max(\omega)$ is maximal frequency to be determined and $\min(V)$ is minimal phase velocity in the considered frequency range, $\min(\omega) \leqslant \omega \leqslant \max(\omega)$. On the other side, the absolute value of wave vector can be evaluated as ($|k|\leqslant K$)

$$|k|\simeq\pi\sqrt{\left(\frac{n_1}{L_1}\right)^2+\left(\frac{n_2}{L_2}\right)^2+\left(\frac{n_3}{L_3}\right)^2}, \qquad (5)$$

where L_j are characteristic dimensions of the sample. If the number of frequencies which have wave vectors inside the sphere Eq. (4) is large enough and all sizes L are of the same order, this coincides with the rule

$$n_1+n_2+n_3\leqslant N, \qquad (6)$$

proposed in Refs. 7 and 5 for a nearly cubic shape. Here N is related to the number of resonance frequencies to be determined: $(N+1)(N+2)(N+3)/6$.

As mentioned, the Lagrangian approach is typically used for such problems. As the Lagrangian $L(a_\gamma)$ is stationary at natural frequencies (a_γ are the complex amplitudes of eigenmodes), all derivatives $\partial L/\partial a_\gamma$ must be zero. As a result, resonance frequencies ω_γ can be determined as a solution for the eigenvalue problem (the notation of Ref. 5 is used):

$$\omega^2\hat{E}_{ik\nu\gamma}a_{k\gamma}=\hat{\Gamma}_{ik\nu\gamma}a_{k\gamma}. \qquad (7)$$

Here the "mass" matrix $\hat{E}$ for a homogeneous sample is defined as follows:

$$\hat{E}_{ik\nu\gamma}=\rho\omega^2\langle\Psi_\nu|\Psi_\gamma\rangle\delta_{ik}. \qquad (8)$$

For a homogeneous sample, the "rigidity" matrix $\hat{\Gamma}$ can be written in the following form:

$$\hat{\Gamma}_{ik\nu\gamma}=\sum_{j,l}^{3}C_{ijkl}b_{jl}(n_1,n_2,n_3|\tilde{n}_1,\tilde{n}_2,\tilde{n}_3). \qquad (9)$$

The values of $\langle\Psi_\nu|\Psi_\gamma\rangle$ and b_{jl} related to the basis functions Ψ_γ are defined in the Appendix for both rectangular and cylindrical geometries of a specimen.

As the tensor C_{ijkl} is symmetrical,[8] the matrix $\hat{\Gamma}$ is symmetrical too. Because the matrix $\hat{E}$ is positive definite, the corresponding eigenvalues of Eq. (7) are real. Then, we can use one of the standard methods to solve the problem in Eq. (7) (see, e.g., Ref. 9).

In what follows we shall use this standard approach for our experiments with RAS of rectangular specimens.

B. Calculation of dissipative parameters

For the materials considered here, due to their complex grainy structure, losses are a very important characteristic

which can, in particular, prevent using high-frequency impulse methods of testing. Usually losses in solids are described by small imaginary parts of elastic moduli. Such a description is valid for a wide range of frequencies[10] and can be invalid only for specific conditions, for example, when grain sizes are compatible with the length of the elastic waves. Therefore, the elastic moduli can be written as follows (the standard double-subscript notation is used below[8]):

$$C_{kl} - i\tilde{C}_{kl} = C_{kl}(1 - i\eta_{kl}), \quad (10)$$

where η_{kl} are small dimensionless parameters representing the internal friction normalized by the elastic constants C_{kl}.

In the paper in Ref. 11, a possible way to determine dissipation parameters was proposed. The main idea of this paper is, in fact, the perturbation method: i.e., to use a RAS solution for a medium without losses as a basic solution and then make corresponding adjustments. The resonance frequency of each mode is a function of the elastic moduli C_{kl}, the size of the sample L_j, and the material density ρ:

$$\omega_n = \omega_n(C_{kl}, L_j, \rho). \quad (11)$$

It is assumed that the functions ω_n of all their arguments in Eq. (11) are regular. Using the Cauchy–Riemann conditions for the complex functions Eq. (11), written separately for each variable, one immediately obtains (all derivatives correspond to $C_{kl}^{(0)}$ that are the solutions of RUS problem without losses):[12]

$$\Delta\omega_n = \sum_{k,l} \left(\frac{\partial\omega_n}{\partial C_{kl}} \Delta C_{kl} - \frac{\partial\tilde{\omega}_n}{\partial C_{kl}} C_{kl}^{(0)} \eta_{kl} \right),$$

$$\tilde{\omega}_n = \sum_{k,l} \left(\frac{\partial\omega_n}{\partial C_{kl}} C_{kl}^{(0)} \eta_{kl} + \frac{\partial\tilde{\omega}_n}{\partial C_{kl}} \Delta C_{kl} \right), \quad (12)$$

where ΔC_{kl} are the adjustments of the real parts of elastic moduli due to losses, $\Delta\omega_n$ is the perturbation of an nth resonance frequency, $\tilde{\omega}_n = \omega_n/2Q_n$, and Q_n is the Q-factor for the frequency ω_n. If $Q_n \gg 1$, all terms in the first equation of Eqs. (12) and, consequently, $\Delta\omega_n$ are of the second order with respect to $\tilde{\omega}_n$. Hence, the change of resonance frequencies due to losses can be neglected. Similarly, the last term in the expression for $\tilde{\omega}_n$ can also be omitted. As a result, the loss factors η_{kl} for the elastic moduli can be determined as a solution of a linear set of equations:

$$\sum_{k,l} \frac{\partial\omega_n}{\partial C_{kl}} C_{kl}^{(0)} \eta_{kl} = \frac{\omega_n}{2Q_n}. \quad (13)$$

For the overdetermined set of equations in Eq. (13), η_{kl} are the medium parameters to be found. The measured values in Eq. (13) are resonance frequencies ω_n and quality factors Q_n. From Eq. (13) one can also predict Q_n using the tensor η_{kl}.

C. Inverse problem

Equations (7) and (13) allow one to solve a general direct problem of resonant acoustic spectroscopy for samples with dissipation. To solve the inverse problem, one should start with a guessed set of elastic constants in the direct problem and then use an iteration procedure to find the set of

constants in question. Random errors can be reduced by using a larger number of measured frequencies and solving a least squares problem. In general, numerous iteration algorithms and fitting criteria can be used to find the best approach for obtaining the values of the elastic constants with the needed accuracy.[13]

The problem is commonly formulated as one of minimization of the mean-square-root difference between the measured and calculated resonance frequencies or, more exactly, of the corresponding functional. The latter can be defined as

$$\varepsilon = \sqrt{\sum_{n=1}^{N} (f_n - \breve{f}_n)^2 \Big/ \sum_{n=1}^{N} (\breve{f}_n)^2}, \quad (14)$$

where f_n are calculated frequencies depending on current values of C_{ijkl}; subscript "n" denotes the number in the list of frequencies (in ascending order); $\breve{f}_n$ are the corresponding measured values of the frequencies. Experimental mode identification can be successfully used to eliminate ambiguity and regular errors in the evaluation of C_{ijkl}.[14] However, such identification is a very complicated problem, and we did not use it here. In this paper we restricted ourselves to the use of Eq. (14) to define fit error in the inverse RAS problem.

The problem of finding medium parameters which minimize the difference between experimental data and calculations can be represented by a system of equations

$$d_l(\mathbf{p}) = 0, \quad l = 1, 2, \ldots, n, \quad (15)$$

where $\mathbf{p} = p_1, \ldots p_n$ is the vector of parameters to be determined. In our case, functions d_l in Eq. (15) are the differences $f_j^{(i)} - \breve{f}_j^{(i)}$. In terms of the extremal problem, the system Eq. (15) is equivalent to the problem of minimization of the function:[15]

$$\mathcal{D}(p_1, p_2, \ldots, p_n) \equiv \sum_{l=1}^{n} |d_l(p_1, p_2, \ldots, p_n)|^2, \quad (16)$$

or of any other monotonically increasing function of $|d_l|$. In particular, the value of ε defined above can also be used as the function $\mathcal{D}$.

To solve the problem Eq. (16) by an iteration method, one should start with some arbitrary values $p_l^{[0]}$. Then sequential approximations are created:

$$p_l^{[k+1]} = p_l^{[k]} + \delta p_l^{[k]}, \quad (17)$$

which should converge to the "exact" values $\mathbf{p}$ when $k \rightarrow \infty$.

To reduce the time of calculations, gradient schemes are usually used. In what follows we use Newton's gradient method. Namely, one finds sequential approximations for $p_l^{[k]}$ as the solution of a set of linear equations:

$$d_l(\mathbf{p}^{[k]}) + \sum_{j=1}^{n} \frac{\partial d_l}{\partial p_j}\bigg|_{\mathbf{p} = \mathbf{p}^{[k]}} \delta p_j^{[k]} = 0. \quad (18)$$

The convergence conditions for procedure Eq. (18) are defined by the Kantorovich theorem.[15]

The number of measured and predicted (from the direct problem) resonance frequencies is typically greater than the

number of parameters to be determined. In this case the solution of Eq. (18) can be obtained as that of the corresponding least squares problem:

$$\delta\mathbf{p} = -(\hat{\mathcal{A}}^T\hat{\mathcal{A}})^{-1}\hat{\mathcal{A}}^T\mathbf{d}, \tag{19}$$

where $\delta\mathbf{p} = \mathbf{p}^{[k+1]} - \mathbf{p}^{[k]}$, $\hat{\mathcal{A}} = (\partial d_l/\partial p_j)$, $\mathbf{d}$ is the vector of functions d_l, and $\hat{\mathcal{A}}^T$ is a transposed matrix. We shall use this scheme in calculations presented below.

D. Test of the code

To verify the workability of our code we applied it to the data given in the book[3] (page 112, data for steel sample 5120). The corresponding parameters are: elastic moduli $C_{11} = 2.7372 \cdot 10^{11}$ Pa, $C_{44} = 8.9190 \cdot 10^{10}$ Pa, density $\rho = 7790$ kg/m^3 and sample size $3.045 \times 2.665 \times 2.645$ mm^3. Data presented in Ref. 3 were obtained for $N = 10$ and the inequality (6) was used. We used the same conditions in our calculations too. The difference in calculated frequencies appears only in sixth digit. Thus our code works as well as that of Ref. 3 for rectangular geometry.

To evaluate this code for cylindrical geometry, we compared its results with analytical models such as Pochgammer-Chree equation[16] for compression modes and Timoshenko's equations for flexural modes.[17] As is well known, these models give a good approximation for long cylindrical bars. Indeed, as a cylinder becomes longer/thinner, the difference between the corresponding asymptotic solutions and numerical calculations becomes negligible (see Ref. 18). Both inequalities (6) and (20) (see the next subsection for the latter) were tested to verify the code for the cylindrical geometry.

E. Modification of RAS method for prolate specimens

To conclude the theoretical part, we suggest a useful modification of RAS that may enable one to significantly save computer time when prolate objects with $L_1 \gg L_{2,3}$ (such as many borehole specimens) are tested. In this case, the use of the condition Eq. (6) that actually supposes that the same-order amount of modal numbers is used for all sides of the sample is excessive, and it is natural to accept the same order of *spatial scale* of the modes for each side to keep the same preciseness. For prolate samples we use the following natural restriction on numbers n_j:

$$\frac{n_1}{L_1} + \frac{n_2}{L_2} + \frac{n_3}{L_3} \leq \frac{N}{\max(L_j)}. \tag{20}$$

To obtain the same resolution in all directions, we keep all three terms in the left-hand part of Eq. (20) comparable in order [this is actually the reason for using $\max(L_j)$ in the right-hand side of that inequality]. As a result, $n_{1,2} \ll n_3$, and instead of a sphere in the n-space it suffices to consider a prolate spheroid of a much smaller volume, practically without an increase in error in comparison with the sphere Eq. (6).
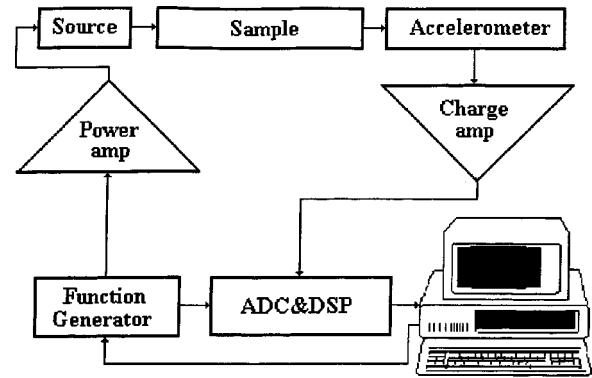

FIG. 1. Block-diagram of experimental setup for measuring the amplitude-frequency response of tested samples. DSP—digital signal processor; ADC—analog-to-digit converter.

III. EXPERIMENTAL SETUP, DATA PROCESSING, AND RESULTS OF MEASUREMENTS

A. Experimental design

The first tested specimen was a black rock of rectangular shape (from Zhitomir, Ukraine). The sizes of the parallelepiped sides were $L_1 = 150.5$ mm, $L_2 = 114.2$ mm, and $L_3 = 102.8$ mm; its mass was $M = 5.435$ kg. The sample had a fine granular structure with no visible flaws.

The block-diagram of the experimental setup for measuring the amplitude-frequency response of tested samples is shown in Fig. 1. A function generator produced a frequency-modulated signal with the frequency swept linearly in time under computer control. After passing a power amplifier, the signal was applied to the transmitting acoustical transducer which excited vibrations in the specimen. The receiving sensor (accelerometer) transformed the specimen vibrations into an electrical signal which was then amplified by a charge amplifier and forwarded to the first input channel of the data acquisition board (ADC&DSP). The transmitting and receiving sensors were thin piezoelectric plates 16 mm in diameter and 2.5 g made of lead zirconate titanate. Epoxy glue was used to attach them to the sample. The electrical signal produced by a function generator was sent to the second channel. Both signals were used for signal processing by a DSP. The signal from the receiving acoustical sensor (accelerometer), after frequency conversion by a function generator and subsequent narrow-band filtering, was recoded into real–imaginary form and sent to the hard disk together with the corresponding frequencies. The total sweep time was chosen according to the Q-factor values to record all peaks with high accuracy. The Q-factors were about 10^3 for measured modes so that all resonant peaks were resolved quite well. In this case the positions of maximums coincide well with resonance frequencies, and the Q-factor for each peak could be defined from the peak width. In Fig. 2 the amplitude-frequency response of the rock is shown on a log-lin scale. To reduce the influence of supports, the sample was hung on thin threads. Simple evaluation of the resonances of the threads gives resonance frequencies of about 0.04 Hz for transverse ("pendulumlike") motions and about 4 Hz for vertical oscillations (due to thread elasticity). Also the effect of transducer masses on resonance frequencies was estimated
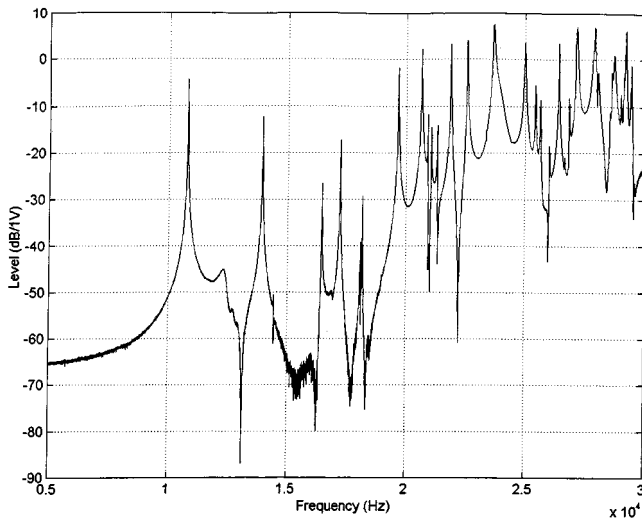
Ostrovsky *et al.*: Resonant acoustic spectroscopy for rock   1773

FIG. 2. Amplitude-frequency response of the rock sample.

FIG. 4. Amplitude-frequency response of the brick obtained for transmitter in position 5 and receiver in position 2.

to not exceed a fraction of a percent. Therefore, at the frequencies of 3 to 20 kHz used in the experiments, free boundary conditions can be considered as a good approximation.

The second sample tested as an example of a building material was a standard ceramic brick of rectangular shape, having a lower Q-factor (that is closer to that of some sandstone-type rocks). The sizes of the parallelepiped were $L_1 = 250$ mm, $L_2 = 125$ mm and $L_3 = 85$ mm; the mass was $M = 5$ kg. This sample had larger grains than the first one, also with no visible flaws.

To excite and measure all oscillation modes in the brick, we put five small sensors to positions shown in Fig. 3. Because of lower values of the Q-factor, several positions of the emitter and receiver were used to resolve all resonant frequencies within the frequency band of interest. The third and the fifth of the sensors were used to excite acoustic vibrations in the brick and the others to receive them. The transmitting and receiving sensors are piezoelectric plates (20 mm in diameter and 1 mm thick) made of lead zirconate titanate. Epoxy glue was used to attach them to the sample. Similarly to the first sample, the brick was hung on thin threads. For example, in Fig. 4 we show the amplitude-frequency response of the brick excited by the transmitter in position 5 and measured by the receiver in position 2 (see Fig. 3).

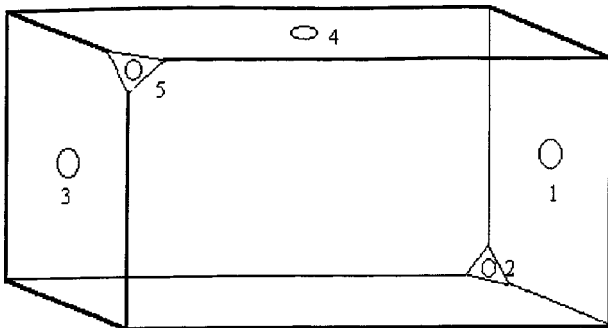Resonant frequencies and corresponding Q-factors were associated with local maxima in the amplitude-frequency re-
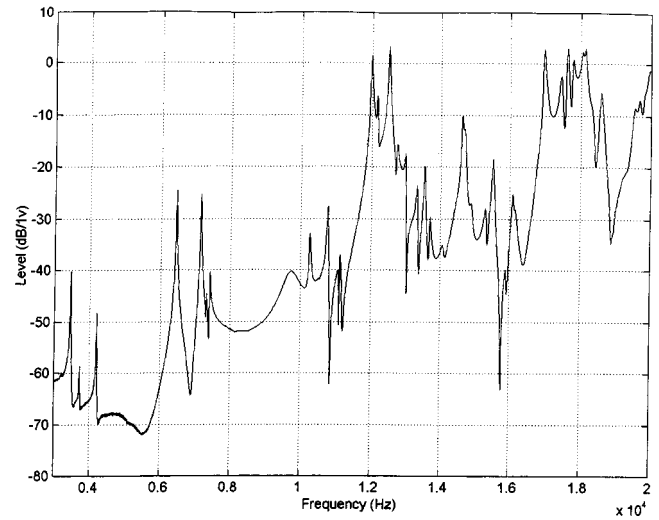

FIG. 3. Sensor positions for experiments with the brick.

sponse. We picked all local maxima in the amplitude-frequency response which exceeded the background level by 2–3 dB and more (as seen from Figs. 2 and 4, in most cases this ratio was much larger). To measure the Q-factors, we used the vicinity of a resonance maximum and represented this vicinity by a standard Lorentz shape. Taking advantage of several transmitters and receivers, for each resonance the amplitude-frequency response was chosen which gives the largest signal/background ratio.

The corresponding frequencies and Q-factors of the vibrations in the samples were calculated according to the scheme described above. Tables I and II demonstrate the results for the rock sample. Tables III and IV demonstrate the results for the ceramic brick.

B. Elasticity and loss parameters of the tested samples

A comparison of measured and calculated frequencies and Q-factors for the rock sample is given in Table I. The mean-square-root difference between measured and calculated frequencies is 0.17%. Such a small error can, at least partly, be caused by the small lumped impedance of the piezo-ceramics transmitters. Indeed, their total mass was approximately 5 g, while the specimen mass was slightly over 5 kg. According to the estimate, the maximal frequency shift due to the lumped impedance can reach 0.1%. We considered this fit error as small enough, and no special procedures were undertaken to reduce this effect.

The results of inverse RAS problem solution are shown in Table II. To start the iterations for the elastic modulus, we performed special pulse-delay measurements for the compressional wave (the result is $C_l \approx 6380$ m/s), whereas the initial value of the Poisson ratio ($\nu \approx 0.1$) was taken from standard tables[19] to define the shear modulus.

The sample has parameters which are rather close to a basalt from the mantle top:[20] $C_{11} = 0.81$ to 1.04×10^{11} N/m^2, $C_{44} = 3 \times 10^{10}$, Poisson ratio $\nu = 0.23$ and density $\rho = 3300$ kg/m^3. This seems to agree with the fact that

TABLE I. Calculated and measured frequencies and Q-factors for a rectangular rock specimen of $150.5 \times 114.2 \times 102.8$ mm^3 having a 5.435 kg mass and considered isotropic. The number of polynomials is limited by $N=13$ with the constraint Eq. (6). Q-factors were calculated from Eq. (13) after finding the η's.

	Frequencies (kHz)		Error	Q-factors		Error
#	Calc.	Meas.	%	Calc.	Meas.	%
1	10.8051	10.8020	+0.03	1304	1441	−9.48
2	13.9212	13.9510	−0.21	1221	1601	−23.8
3	14.4560	14.4570	−0.01	1215	1415	−14.1
4	16.5271	16.4760	+0.31	1303	1546	−15.7
5	17.1951	17.2460	−0.29	1292	1360	−5.02
6	18.1429	18.1350	+0.04	1261	1128	+11.8
7	18.1692	18.1820	−0.07	1291	1256	+2.76
8	19.7260	19.6780	+0.24	1265	1513	−16.4
9	20.5777	20.6520	−0.36	1162	1311	−11.4
10	20.8999	20.9100	−0.05	1270	1016	+25.0
11	21.0045	21.0200	−0.07	1265	1335	−5.28
12	21.2718	21.2630	+0.04	1281	1291	−0.81
13	21.9518	21.8910	+0.28	1285	1255	+2.40
14	22.5604	22.5800	−0.09	1218	1280	−4.84
15	23.3352	23.3670	−0.14	1292	1461	−11.6
16	23.6955	23.7150	−0.08	1193	1444	−17.4
17	25.0200	25.0050	+0.06	1226	1064	+15.2
18	25.4484	25.4000	+0.19	1149	934	+23.0
19	25.6512	25.6350	+0.06	1110	1188	−6.53
20	26.0721	26.0650	+0.03	1260	1145	+10.0
21	26.4261	26.4430	−0.06	1298	1243	+4.42

the corresponding site lies on the Ukraine's shield known to have reached a very shallow area.

For comparison we performed the same procedure supposing that the specimen's material is anisotropic with cubic symmetry. As there were no *a priori* data regarding symmetry axes, we aligned them along the specimen axes. From Table II it is seen that error remains of the same order as for an isotropic sample model. As there is no evident physical reason for any systematic anisotropy, it can be concluded that the sample is isotropic.

The values of the Q-factor have greater dispersion than those of resonance frequencies. This seems natural because the measured Q is found from the widths of the corresponding resonance curves that are "contaminated" by neighboring resonances. Factors such as sound radiation into air may

TABLE II. The results of an inverse problem solution for the rock specimen. Values of δF and δQ were obtained as relative rms errors of the fits. ΔC_{ij} are errors which correspond to obtained δF.

	Isotropic specimen	Cubic anisotropy
C_l (m/s)	6366	6363
C_t (m/s)	3592	3590[a]
ν	0.27	—
C_{11} GPa	$124.6 \cdot (1-0.0011i)$	$124.5 \cdot (1-0.0011i)$
C_{12} GPa	$45.25 \cdot (1-0.0016i)$	$45.06 \cdot (1-0.0017i)$
C_{44} GPa	$39.70 \cdot (1-0.0008i)$	$39.66 \cdot (1-0.0008i)$
δF (%)	0.17	0.17
δQ (%)	13.3	13.3
ΔC_{11} GPa	2.10	0.39
ΔC_{12} GPa	2.39	0.44
ΔC_{44} GPa	0.14	0.23

[a]Along the main crystal axis "100."

TABLE III. The results of an inverse problem solution for a ceramic brick of $250 \times 125 \times 85$ mm^3 size and 5 kg mass considered isotropic. Values δF and δQ were obtained as relative rms errors of the fits. ΔC_{ij} are errors corresponding to obtained δF.

C_l (m/s)	3305.4
C_t (m/s)	2155.1
ν	0.13
C_{11} GPa	$21.4 \cdot (1-0.0040i)$
C_{44} GPa	$9.11 \cdot (1-0.0036i)$
δF (%)	0.59
δQ (%)	21.3
ΔC_{11} GPa	1.08
ΔC_{44} GPa	0.17

also be significant. A simple estimate shows that at the frequency of 10 KHz, the radiation alone limits the Q-factor by a maximum of about 10^4. The corresponding error is comparable with the values given in Table II.

The results of inverse RAS problem solution for the brick are shown in Tables III and IV. One can see a good correspondence between measured and calculated resonance frequencies. The errors in Q are larger in comparison with the first sample. As the values of the Q-factor are typically 3–4 times less than those for the rock sample, these errors can be due to interference of neighboring resonances. Some ways to better resolve interferring resonances is the subject of our present research.

Data in parentheses in Table IV correspond to the results

TABLE IV. Calculated and measured frequencies and Q-factors for a ceramic brick considered isotropic. The order of the polynomials was limited by $N=17$ with the constraint Eqs. (6) and, for data in parentheses, (20).

	Frequencies (kHz)		Error
#	Calc.	Meas.	%
1	3.466 60(3.466 54)	3.466 30	+0.01(+0.01)
2	3.717 01(3.717 02)	3.732 80	−0.42(−0.42)
3	4.187 72(4.187 65)	4.209 40	−0.51(−0.52)
4	6.460 20(6.460 09)	6.439 70	+0.32(+0.32)
5	7.165 39(7.165 32)	7.138 00	+0.38(+0.38)
6	7.291 85(7.291 93)	7.309 40	−0.24(−0.24)
7	7.428 62(7.428 54)	7.409 80	+0.25(+0.25)
8	10.2172(10.2174)	10.2780	−0.59(−0.59)
9	10.4107(10.4108)	10.5400	−1.23(−1.23)
10	10.8838(10.8837)	10.7870	+0.90(+0.90)
11	10.9152(10.9151)	10.8540	+0.56(+0.56)

	Q-factor		Error
#	Calc.	Meas.	%
1	+262.52(+262.53)	227.70	+15.29(+15.30)
2	+279.56(+279.55)	267.20	+4.62(+4.62)
3	+263.08(+263.09)	271.80	−3.21(−3.21)
4	+262.28(+262.29)	387.20	−32.26(−32.26)
5	+266.64(+266.64)	358.70	−25.67(−25.66)
6	+278.38(+278.37)	314.60	−11.51(−11.51)
7	+270.85(+270.85)	336.40	−19.49(−19.49)
8	+264.01(+264.02)	231.00	+14.29(+14.30)
9	+276.06(+276.06)	309.00	−10.66(−10.66)
10	+274.90(+274.89)	316.00	−13.01(−13.01)
11	+272.74(+272.74)	188.00	+45.07(+45.07)

of calculations according to the code modified for prolate samples. It is noteworthy that the use of the constraint Eq. (20) instead of Eq. (6) enables us to reduce the time of calculations by a factor of 10 with practically the same accuracy, even for the brick in which the ratio of different sides does not exceed 3.

IV. CONCLUSIONS

This paper demonstrates that the method of resonant acoustic spectroscopy can be effectively applied to large specimens of structurally inhomogeneous materials such as rocks and ceramics. After Birch who also worked with large specimens, we utilized the more recently developed RUS algorithms and applied them to large rectangular specimens. Note that the numerical program created and used here can be applied to anisotropic samples as was demonstrated above on a simple example of cubic symmetry. Also, a modification of the method significantly reducing the numerical time for prolate samples has been suggested and verified. We suppose that a further development will result in creating practical tools for testing borehole samples and industrial materials, including those with defects.

ACKNOWLEDGMENT

APPENDIX: MASS AND RIGIDITY MATRIX ELEMENTS

As both cylindrical bars and rectangular parallelepipeds are important from the point of view of their practical application, both these cases are considered here.

Cylindrical shape:

$$\langle \Psi_\nu | \Psi_\gamma \rangle = \mathcal{P}(n_1 + \tilde{n}_1, n_2 + \tilde{n}_2, n_3 + \tilde{n}_3), \tag{A1}$$

where the functions $\mathcal{P}(\cdots)$ are defined as

$$\mathcal{P}(\alpha_1, \alpha_2, \alpha_3) = \begin{cases} \dfrac{2R^2 H}{(\alpha_2 + 1)(\alpha_3 + 1)} \cdot \dfrac{\Gamma\left(\dfrac{\alpha_1 + 1}{2}\right)\Gamma\left(\dfrac{\alpha_2 + 3}{2}\right)}{\Gamma\left(\dfrac{\alpha_1 + \alpha_2}{2} + 2\right)} \\ \qquad \alpha_1, \alpha_2 \text{ are even} \\ 0 \quad \text{otherwise,} \end{cases} \tag{A2}$$

and $\Gamma(\ldots)$ is the gamma function, R is the radius of a cylinder and H is its length.

Values of $b_{ij}(\cdots|\cdots)$ are defined as follows:

$$b_{11} = n_1 \tilde{n}_1 \mathcal{P}(n_1 + \tilde{n}_1 - 2, \quad n_2 + \tilde{n}_2, \quad n_3 + \tilde{n}_3),$$

$$b_{12} = n_1 \tilde{n}_2 \mathcal{P}(n_1 + \tilde{n}_1 - 1, \quad n_2 + \tilde{n}_2 - 1, \quad n_3 + \tilde{n}_3),$$

$$b_{13} = n_1 \tilde{n}_3 \mathcal{P}(n_1 + \tilde{n}_1 - 1, \quad n_2 + \tilde{n}_2, \quad n_3 + \tilde{n}_3 - 1),$$

$$b_{21} = n_2 \tilde{n}_1 \mathcal{P}(n_1 + \tilde{n}_1 - 1, \quad n_2 + \tilde{n}_2 - 1, \quad n_3 + \tilde{n}_3),$$

$$b_{22} = n_2 \tilde{n}_2 \mathcal{P}(n_1 + \tilde{n}_1, \quad n_2 + \tilde{n}_2 - 2, \quad n_3 + \tilde{n}_3), \tag{A3}$$

$$b_{23} = n_2 \tilde{n}_3 \mathcal{P}(n_1 + \tilde{n}_1, \quad n_2 + \tilde{n}_2 - 1, \quad n_3 + \tilde{n}_3 - 1),$$

$$b_{31} = n_3 \tilde{n}_1 \mathcal{P}(n_1 + \tilde{n}_1 - 1, \quad n_2 + \tilde{n}_2, \quad n_3 + \tilde{n}_3 - 1),$$

$$b_{32} = n_3 \tilde{n}_2 \mathcal{P}(n_1 + \tilde{n}_1 - 1, \quad n_2 + \tilde{n}_2 - 1, \quad n_3 + \tilde{n}_3),$$

$$b_{33} = n_3 \tilde{n}_3 \mathcal{P}(n_1 + \tilde{n}_1, \quad n_2 + \tilde{n}_2, \quad n_3 + \tilde{n}_3 - 2).$$

In the case of *rectangular shape* it is better to use a Legendre polynomial expansion in the Ritz representation Eq. (3). In this case the values of interest are written as follows (L_1, L_2, L_3 are sizes of a rectangular specimen):

$$\langle \Psi_\nu | \Psi_\gamma \rangle = \frac{L_1 L_2 L_3 \delta_{\nu\gamma}}{(2n_1 + 1)(2n_2 + 1)(2n_3 + 1)}, \tag{A4}$$

and

$$b_{11} = \frac{2\delta_{n_2 \tilde{n}_2} \delta_{n_3 \tilde{n}_3}}{(2n_2 + 1)(2n_3 + 1)} \frac{L_2 L_3}{L_1} G_{n_1 \tilde{n}_1},$$

$$b_{12} = \frac{\delta_{n_3 \tilde{n}_3}}{2n_3 + 1} L_3 F_{\tilde{n}_1 n_1} F_{n_2 \tilde{n}_2},$$

$$b_{13} = \frac{\delta_{n_2 \tilde{n}_2}}{2n_2 + 1} L_2 F_{\tilde{n}_1 n_1} F_{n_3 \tilde{n}_3},$$

$$b_{21} = \frac{\delta_{n_3 \tilde{n}_3}}{2n_3 + 1} L_3 F_{n_1 \tilde{n}_1} F_{\tilde{n}_2 n_2},$$

$$b_{22} = \frac{2\delta_{n_1 \tilde{n}_1} \delta_{n_3 \tilde{n}_3}}{(2n_1 + 1)(2n_3 + 1)} \frac{L_1 L_3}{L_2} G_{n_2 \tilde{n}_2}, \tag{A5}$$

$$b_{23} = \frac{\delta_{n_1 \tilde{n}_1}}{2n_1 + 1} L_1 F_{\tilde{n}_2 n_2} F_{n_3 \tilde{n}_3},$$

$$b_{31} = \frac{\delta_{n_2 \tilde{n}_2}}{2n_2 + 1} L_2 F_{n_1 \tilde{n}_1} F_{\tilde{n}_3 n_3},$$

$$b_{32} = \frac{\delta_{n_1 \tilde{n}_1}}{2n_1 + 1} L_1 F_{n_2 \tilde{n}_2} F_{\tilde{n}_3 n_3},$$

$$b_{33} = \frac{2\delta_{n_1 \tilde{n}_1} \delta_{n_2 \tilde{n}_2}}{(2n_1 + 1)(2n_2 + 1)} \frac{L_1 L_2}{L_3} G_{n_3 \tilde{n}_3},$$

with

$$F_{mn} = \begin{cases} 2, & n > m \text{ and } n + m \text{ is odd,} \\ 0, & \text{otherwise,} \end{cases}$$

$$G_{mn} = \begin{cases} (\min(m,n)) \cdot (\min(m,n) + 1), & n + m \text{ is even,} \\ 0 & \text{otherwise.} \end{cases} \tag{A6}$$

[1] G. Mavko, T. Mukeji, and J. Dvorkin, *The Rock Physics Handbook. Tools For Seismic Analysis in Porous Media* (Cambridge University Press, Cambridge, MA, 1998).

[2] J. E. White, *Underground Sound, Application of Seismic Waves* (Elsevier, New York, 1983).

[3] A. Migliori and J. L. Sarrao, *Resonant Ultrasound Spectroscopy* (Wiley, New York, 1998).

[4] F. Birch, "Velocity and attenuation from resonant vibrations of spheres of rock, glass, and steel," J. Geophys. Res. **80**, 756–764 (1975).

[5] W. Visscher, A. Migliori, T. Bell, and R. Reinert, "On the normal modes of free vibrations of inhomogeneous and anisotropic elastic objects," J. Acoust. Soc. Am. **90**, 2154–2162 (1991).

[6] I. Ohno, "Free vibration of a rectangular parallelepiped crystal and its

1776   J. Acoust. Soc. Am., Vol. 110, No. 4, October 2001

Ostrovsky *et al.*: Resonant acoustic spectroscopy for rock

application to determination of elastic constants of orthorhombic crystals," J. Phys. Earth **24**, 355–379 (1976).

[7] H. Demarest, "Cube-resonance method to determine the elastic constants of solids," J. Acoust. Soc. Am. **49**, 768–775 (1971).

[8] L. D. Landau, E. M. Lifshitz, A. M. Kosevich, and L. P. Pitaevskii, *Theory of Elasticity* (Pergamon, New York, 1986).

[9] J. H. Wilkinson and C. Reinsch, *Handbook for Automatic Computation, Vol. 2, Linear Algebra* (Springer-Verlag, New York, 1971).

[10] A. D. Nashif, D. I. G. Johnes, and J. P. Henderson, *Vibration Damping* (Wiley, New York, 1985).

[11] Y. Sumino, I. Ohno, and M. Kumazawa, "Measurement of elastic constants and internal frictions on single-crystal MgO by rectangular parallelepiped resonance," J. Phys. Earth **24**, 263–273 (1976).

[12] B. V. Shabat, *Introduction in Complex Analysis, Vol. 2, Functions of Several Variables*, 3rd edition [in Russian] (Nauka, Moscow, 1985).

[13] R. W. Hamming, *Numerical Methods for Scientists and Engineers* (Bell Telephone Laboratories, McGraw-Hill, New York, 1962).

[14] J. Maynard, "Resonant ultrasound spectroscopy," Phys. Today **27**, 26–32 (1996).

[15] G. A. Korn and T. M. Korn, *Mathematical Handbook for Scientists and Engineers*, 2nd ed. (McGraw-Hill, New York, 1968).

[16] J. N. Sneddon and D. S. Berry, *The Classical Theory of Elasticity* (Springer-Verlag, New York, 1958).

[17] M. C. Junger and D. Feit, *Sound, Structures and Their Interactions*, 2nd ed. (MIT Press, Cambridge, MA, 1986).

[18] A. V. Lebedev, L. A. Ostrovsky, I. A. Soustova, Calculation of natural frequencies for a solid cylinder, Project No. F37750018-35, Technical report 2.6.6, Institute of Applied Physics (Russia)—LANL (USA), 1998.

[19] *Handbook of Physical Values*, edited by acad. I. K. Kikoin (Atomizdat, Moscow, 1976).

[20] *Encyclopedia Britannica*, CD-version 1997, Tables 35, 36.